RSC Advances

ROYAL SOCIETY OF CHEMISTRY

www.rsc.org/advances

RSC Advances

RSCPublishing

ARTICLE

Polyurea dendrimer for efficient cytosolic siRNA delivery

Cite this: DOI: 10.1039/xoxxoooooox

Rita B. Restani,[a] João Conde,[b,c,d] Pedro V. Baptista,[b] Maria Teresa Cidade,[e] Ana M. Bragança,[f] Jorge Morgado,[f,g] Ilídio J. Correia,[h] Ana Aguiar-Ricardo [a,*] and Vasco D. B. Bonifácio[f,*]

Received ooth January 2014,
Accepted ooth January 2014

DOI: 10.1039/xoxxoooooox

www.rsc.org/

The design of small interfering RNA (siRNA) delivery materials showing efficacy in vivo is at the forefront of nanotherapeutics research. Polyurea (PURE-type) dendrimers, are 'smart' biocompatible 3D polymers that unveil a dynamic and elegant back-folding mechanism involving hydrogen bonding between primary amines at the surface and tertiary amines and ureas at the core. Similarly to a biological proton pump, they are able to automatically and reversibly rework their conformation in response to pH stimulus. Herein, we show that PURE-G4 is an useful gene silencing platform showing no cellular toxicity. As a proof-of-concept we investigated the PURE-G4-siRNA dendriplex, which showed to be an attractive platform with high transfection efficacy. The simplicity associated to the complexation of siRNA with polyurea dendrimers makes them a powerful tool for efficient cytosolic siRNA delivery.

1. Introduction

Among anticancer agents, siRNA has emerged as a powerful tool to block gene function via sequence-specific post-transcriptional gene silencing.[1-3] To reach the cytoplasm and interact with the RNAi machinery, naked siRNA need to transpose several physiological barriers since they are highly hydrophilic to cross the cell membrane, show poor chemical stability and low protection against serum nucleases leading to low blood plasma half-life circulation.[4-6] Over the last two decades numerous polymeric and lipophilic vectors had been developed, yet only a small fraction prospered to clinical trials[7] and none of these vectors have received FDA approval.[8]

The unique 3D architecture of dendrimers renders these polymers remarkable structures for enhanced solubilization and controlled release of molecular guests. As a consequence of its unimolecular structure, in cases where dendritic motifs are capable of hydrogen bonding, both shell and core can assume a restricted mobility where the system guest-in-box[9] shows efficient applications in Nanomedicine.[10-14] Despite being the most described dendrimer structures in the literature, poly(amido amine) (PAMAM-type) amine-terminated dendrimers have been reported to exhibit cytotoxicity as a consequence of positive charged surface. Remarkably, we recently reported that polyurea (PURE-type) amine-terminated dendrimers[15] are non-cytotoxic, biodegradable, biocompatible, fluorescent and have high transfection efficiency in human fibroblasts, showing cytoplasmic distribution. Although charge is undoubtedly a general parameter associated with cytotoxicity, several other properties including charge density, morphology, biodegradability, flexibility, molecular weight and amphipathic character are likely relevant to dictate biocompatibility.[16,17] Herein, we scrutinized the chemistry of PURE-type dendrimers in order to fully understand the factors governing self-assembly processes upon different stimuli so as to understand their potential for intracellular trafficking, thus providing a strategy for efficient cellular uptake and subsequent enhancement of lysosomal/endosomal siRNA escape.

2. Results and discussion

The intramolecular back-folding in different dendrimer systems is well described in literature.[18-22] Regarding PAMAM dendrimers, theoretical[23] and experimental data using pH[24] and ^{1}H NMR[25,26] studies support a solvent-dependent "conformational dance".

In the case of PURE dendrimers a more effective intramolecular back-folding is expected due to the strength of urea hydrogen bonding. Indeed, their IR spectra[15] suggest a rigid well-organized core structure due to bidentate hydrogen bonding between urea motifs (1638-1644 cm^{-1}) and absence of free urea carbonyl groups (ca. 1690 cm^{-1}). A similar analysis of urea N-H stretching modes also supports that the observed hydrogen bonding correlates well with bidentate arrangements

(3332-3347 cm^{-1}) without free N-H urea groups (*ca*. 3450 cm^{-1}).[27,28]

Considering the challenges before reaching the target, it is mandatory to explore the multi physico-chemical properties of the carriers in aqueous solution by mimicking the cell and endosomal environment, thus providing relevant insights into drug delivery events. Therefore, we systematically studied the behavior of PURE-type dendrimers at various protonation levels. To predict the intramolecular behaviour upon different pH values, the ^{1}H NMR spectrum of the fourth generation polyurea dendrimer (PURE-G4) was acquired in D_2O (pH 11.55) and the solution was then acidified with DCl (pH 1.77), and finally brought to the initial pH using NaOD (Fig. 1).

The aqueous solutions of PURE dendrimers are strongly basic due to the high content of tertiary amines in the backbone. The spectra show that a reversible protonation process occurs upon acidification-basification (Fig. 1A and 1B), revealing that the medium pH strongly impacts the dendrimers conformation. The ethylene protons from the tertiary amine core showed a very large downfield shift ($\Delta\delta$= 0.90 ppm), and are the most affected upon protonation (Fig. 1, a and a') when compared with the ethylene protons near the urea groups (Fig. 1, b and b'), which are slightly upfield shifted ($\Delta\delta$= 0.11 and $\Delta\delta$= 0.20 ppm).

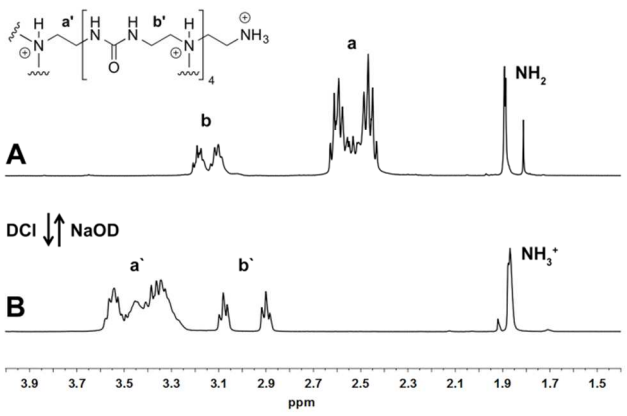

Fig. 1. ^{1}H NMR titration of the PURE-G4 dendrimer: PURE-G4 spectra in D2O and after addition of NaOD (A), and after addition of DCl (B). The chemical structure of protonated PURE-G4, with the attributed chemical shifts (a' and b') in spectrum B, is shown at the top. Chemical shifts of protons a and b in spectrum A correspond to neutral PURE-G4 species.

Atomic force microscopy (AFM) was used to study morphology and film properties.[29] For film preparation, two concentrations (17.5 and 8.5 nM) and two methods (spin-coating and dropcast) were used, and best results were obtained by dropcast in mica plates using 8.35 nM aqueous solutions (pH 7). Although AFM images show equivalent noise, irregular aggregates of ~20 nm were observed (Supporting Information, Fig. S1). The low resolution and aggregation factor did not allow further assessment concerning changes to dendrimer size with pH. Further dimensional characterization and evaluation of pH influence on morphology was investigated via Dynamic Light Scattering (DLS) at different pHs. However, no reproducible results were obtained for aqueous solutions with dendrimer concentrations in the range 1-100 mg/mL, which precluded further analysis, due to the formation of aggregates. The degree of protonation was determined by titration and the values of pK_{a1}= 4.98 and pK_{a2}= 9.78 for tertiary and primary amines, respectively, were obtained (Fig. S2A). The isoelectric point was found at pH 6.62 (Fig. S2). These pH-dependent conformations, owed to protonation and urea-assisted neutralization events, are characteristic of polyurea dendrimers and are schematically represented in Fig. 2. This protonation mechanism resembles proteins 'unfolding' in response to the properties of the surrounding media.[30]

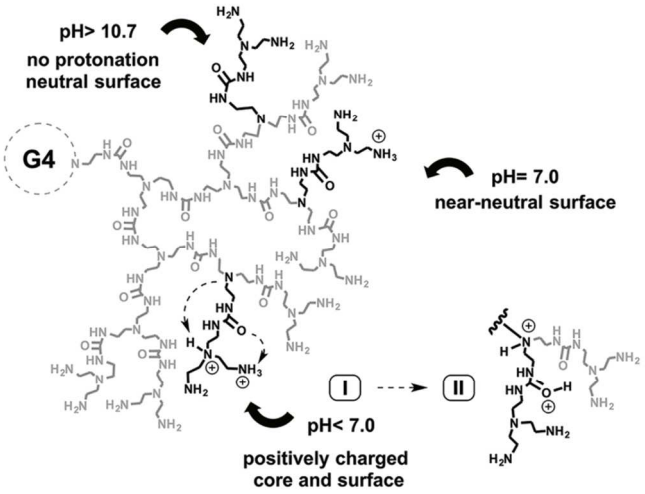

Fig. 2. Schematic representation of the PURE dendritic system at different protonation levels.

As expected, the rheological properties are highly dependent on the capability to establish intramolecular interactions through hydrogen bonding. Fig. S3 in Supporting Information shows that an increase on temperature causes a decrease of dendrimer viscosity, suggesting that intramolecular H-bonds are partially weakened reducing friction between neighbouring molecules, and consequently the viscosity. This supports the observed h_d differences at 25 and 37 ºC, 3.41 and 5.61 nm, respectively. Data also showed that (highly basic) PURE-type dendrimers hold a cationic nature (Fig. 3A), confirming that PURE-G4 has a higher electrophoretic mobility than PAMAM-G4 amine-terminated dendrimer, which can translate the lower Mw of the former. Taken together, the cationic surface of the dendritic system, the pH-dependent flexible structure and the high buffering capacity in the pH range of the endosome, we propose that PURE-G4 present ideal features as a siRNA delivery platform.[31] It is well known that cationic dendrimers can complex with DNA or RNA (i.e. siRNA) via electrostatic interactions.[32,33] We envisaged that electrostatic interactions between the positively charged terminal amines from polyurea dendrimers and the negatively charged siRNA phosphate groups could easily be established. Consequently, an electrophoretic mobility shift assay (EMSA) was performed on agarose gel using increasing concentrations of PURE-G4 (1, 2.5, 5 and 7.5 mg/mL), previously incubated with 10 μM of

siRNA, Fig. 3B and 3C. The relative electrophoretic mobility (RF) for PURE-G4 complexed with siRNA (polyurea dendriplexes) clearly demonstrate that as the mass of PURE-G4 increases, retardation in electrophoretic mobility of siRNA occurs, suggesting successful complexation between both (Fig. 3D). A binding efficiency of ca. 95% was achieved.

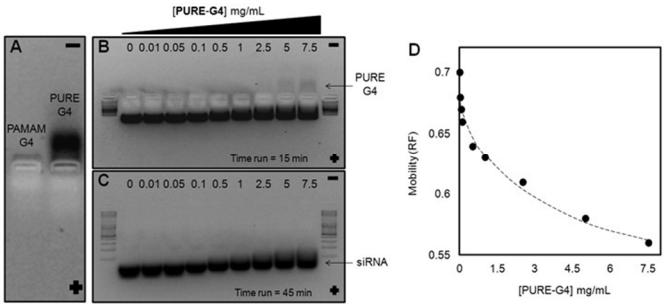

Fig. 3. Photographs of EMSA gel after electrophoresis of PAMAM and PURE-G4 dendrimers (**A**) and increasing amounts of PURE-G4 complexed with 10 μM of siRNA (**B, C**). Determination of the mobility (RF) values for dendriplexes (**D**). RF= distance migrated/gel length. Graph shows electrophoretic mobility in function of PURE-G4 concentration.

To evaluate cell toxicity of the dendriplexes, we assessed cell survival rates of HepG2 cells via the [3-(4,5-dimethylthiazol-2-yl)-2,5-diphenyltetrazoliumbromide] (MTT) reduction assay. PURE-G4 (1, 2.5, 5 and 7.5 mg/mL) and dendriplexes (prepared from the incubation of 1, 2.5, 5 and 7.5 mg/mL of PURE-G4 with 10 nM of siRNA) were used. PURE-G4 showed a reduction in cell viability upon 2.5 mg/mL. Contrarily to what was observed for PURE-G4, no cell cytotoxicity was detected up to 48 h incubation with polyurea dendriplexes even at high PURE-G4 concentrations (Fig. 4A), clearly demonstrating the biological benefits of such complexation. The great differences on the toxicity may be justified based on the charge neutralization resultant from the complexation between the negatively charge backbone from siRNA phosphate groups and positively charged PURE-G4. These findings are in agreement with the neutral zeta potential value obtained for the complex (1.4 ± 0.3). Comparison between cell viability of PURE-G4 and PURE-G4-siRNA complexes and the commercial delivery vector Lipofectamine can be found in Supporting Information, Fig. S4.

Regarding oxidative stress, the glutathione-S-transferase (GST) activity assay showed that PURE-G4 caused extensive glutathione depletion, thus extensive oxidative damage. This behavior was observed as from 2.5 mg/mL of PURE-G4 resulting in ~30%, 50% and 75% reduction in GST activity, respectively (Fig. 4B). MTT and GST activity assay, however, revealed that PURE-type dendriplexes are highly biocompatible in the studied concentration range.

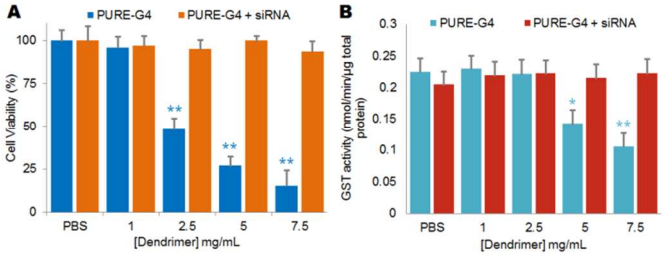

Fig. 4. Cytotoxicity via the MTT assay (**A**) and oxidative stress through the GST activity assay (**B**) of PURE-G4 (1, 2.5, 5 and 7.5 mg/mL) and PURE-G4 complexed with siRNA (1, 2.5, 5 and 7.5 mg/mL of dendrimer pre-incubated with 10 μM of siRNA) administered to human hepatocellular liver carcinoma cells (HepG2) at 48 hours of exposure (*, P<0.05; **, P <0.001).

The 'smart' behavior of polyurea dendrimers, basically governed by their ability to establish reversible hydrogen bonding as an adaptation to stimuli, disclosed a strategic conformational performance for a conceivable efficient sequestration of the polyurea dendriplex system (Fig. 5A) into the cell, mediated by endocytosis pathways (Fig. 5B).

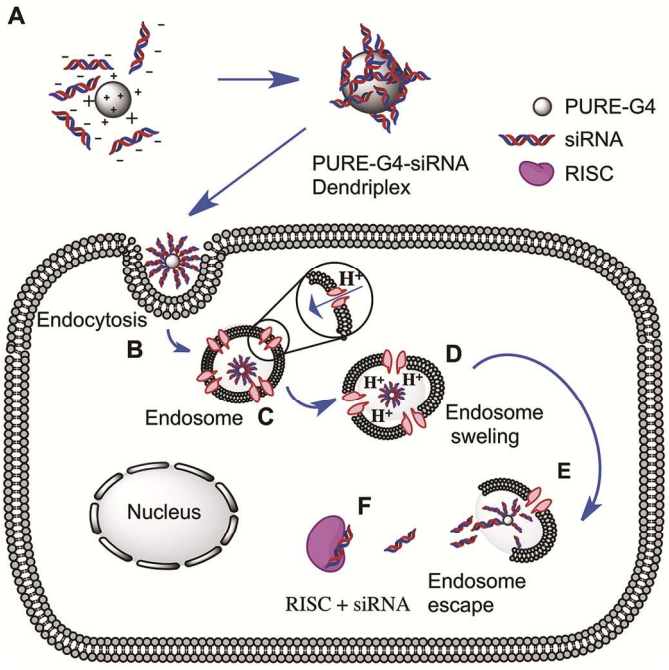

Fig. 5. Schematic representation of PURE-G4 and siRNA complexation in solution (A); Endocytosis (B); Endosome acidification due to proton sponge effect (C) followed by endosome swelling (D); membrane disruption (E) and siRNA loading into RISC (F) for gene silencing. RISC= RNA interference silencing complex.

The acquired results lead us to believe, that as claimed in literature,[34,35] the cocktail of amines (primary and tertiary) and ureas present in the same nano-vehicle may be able to buffer the acidic environment within the endosome. As such, to re-establish the endosomal environment a titrable process is likely to occur, mainly due to a "proton sponge" mechanism,[36,37] in order to lower the cells pH. At pH 5, the buffering capacity of the carrier system (Fig. 5C) will induce the proton sponge

effect and induce swelling of the dendrimer with concomitant endosomal disruption (Fig. 5D and 5E). These events would cause the dendriplex to be released in the reductive environment of the cytosol where siRNA can be easily cleaved into the cytosol, allowing for incorporation into the RNAi pathway (e.g. RISC incorporation),[38] Fig. 5F, that subsequently promote specific events that trigger silencing of specific genes.[39,40]

To track the intracellular co-localization of PURE-G4 and PURE-G4-siRNA within lysosomes we took profit from the intrinsic fluorescence of PURE-type dendrimers. In order to check dendrimers internalization into the lysosomes we used Lysotracker® Green to label these structures. Confocal microscopy exposed dendrimers entrapment within the lysosomal vesicles (see Fig. 6).

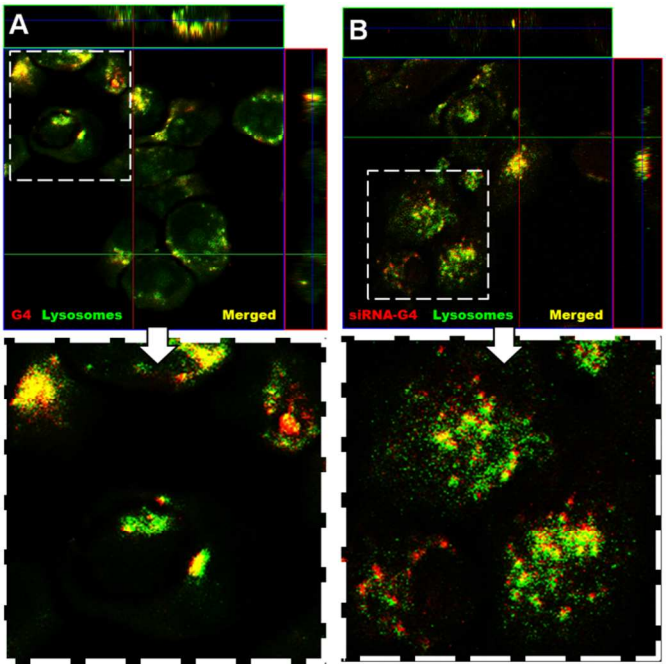

Fig. 6. Intracellular co-localization of PURE-G4 (A) and PURE-G4-siRNA (B) within lysosomes. HepG2 cells were treated with 1mg/mL of PURE-G4 and PURE-G4-siRNA dendrimers (in red) for 48 hours. Lysosomes (in green) were stained with Lysotracker® Green DND26. Overlap of dendrimers and lysosome trackers are represented in yellow in the merged images.

In detail, the co-localization of the tested dendrimers (red dots) within lysosomes (green dots), produced a yellow fluorescence in the merged images, Fig. 6A and 6B. The discrete punctuate appearance of the dendrimer fluorescence and the co-localization of the dendrimer within the lysosome-specific dye insinuated the significant dendrimer uptake into the lysosomes. However, higher internalization efficiency into the lysosome compartment was observed for the free formulation PURE-G4, which has higher hydrophobic character. The PURE-G4-siRNA seemed to escape lysosome more efficiently.

As proof-of-concept, the in vitro potential of the polyurea dendriplex platform was evaluated using HepG2 cells transfected with GFP that was then targeted for silencing with anti-GFP siRNA–PURE-G4 dendriplexes. Cells were treated with several siRNA/PURE-G4 ratios by incubation of different concentrations of PURE-G4 (1, 2.5, 5 and 7.5 mg/mL) with 10 μM of siRNA control or anti-GFP siRNA. After 48 hours, GFP fluorescence of cells treated with anti-GFP dendriplexes was analyzed (Fig. 7) by comparing it with the control (Fig. 7A) using epi-fluorescence imaging.

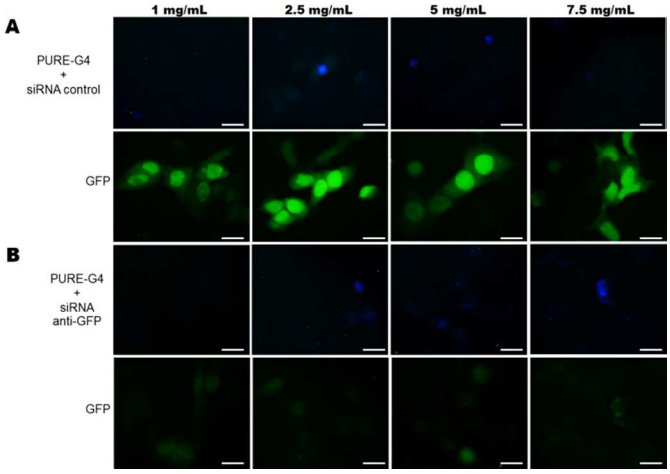

Fig. 7. Representative series of epi-fluorecence images of human hepatocellular liver carcinoma cells (HepG2), 48 hours after incubation with PURE-G4-siRNA dendriplexes (1, 2.5, 5 and 7.5 mg/mL of dendrimer pre-incubated with 10 μM of siRNA control) (A) or anti-GFP siRNA (B). The series of images represents the green fluorescence channels corresponding to GFP fluorescence and the blue fluorescence channels corresponding to PURE-G4 dendriplexes. Scale bars = 20 μm.

The blue fluorescence pattern observed confirmed the PURE-G4 input into the cells and their distribution mainly into the cytoplasm. Concerning GFP fluorescence, it was visually clear that the PURE-type dendriplex induced specific GFP knockdown with an inhibition efficacy of ca. 63% (Fig. 7B), when compared to control siRNA, indicating that the knockdown is sequence specific.

The quantification of GFP expression levels for each formulation is shown in Fig. 8. GFP silencing was confirmed by significant fluorescence decrease from protein in bulk cell lysates (as percentage of original GFP fluorescence levels) only in cells treated with anti-GFP PURE-G4-siRNA dendriplexes (7.5 mg/mL), when compared to control PURE-G4-siRNA dendriplexes and cells with no treatment. A silencing of approximately 80% was achieved for the PURE-type dendriplex, when compared to control siRNA (Fig. 8A). Similar results were achieved for mRNA levels of GFP, using Real-Time RT-PCR (Fig. 8B). Detailed information on primer sequence, cycling conditions and melting analysis about GFP expression assay can be found elsewhere.[41] As for protein level, the mRNA expression reveals an approximately 75% knockdown of GFP with anti-GFP PURE-G4-siRNA dendriplexes (7.5 mg/mL), when compared to control PURE-G4-siRNA dendriplexes. These data discloses that the PURE-G4 siRNA dendriplexes are far more efficient that the commercially transfection agent, Lipofectamine®. Using the

recommended Lipofectamine® concentration for siRNA delivery, we could only achieve ~40% silencing of GFP in the same culturing conditions as for the dendriplexes (see Fig. S5).

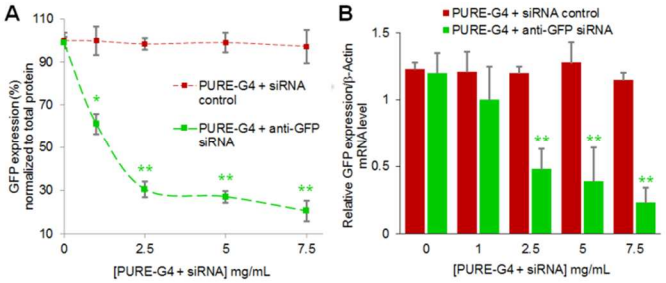

Fig. 8. Quantification of GFP expression levels, 48 hours after incubation with PURE-G4-siRNA dendriplexes (1, 2.5, 5 and 7.5 mg/mL of dendrimer pre-incubated with 10 μM of siRNA control). (A) At the protein level, a knockdown of approximately 80% was achieved for the PURE-type dendriplex, when compared to control siRNA. All GFP expression data was normalized to total protein quantification. (B) At the mRNA level, Real-Time RT-PCR results confirmed GFP knockdown after treatment with increasing amounts of anti-GFP PURE-G4-siRNA and control PURE-G4-siRNA dendriplexes using β-actin as reference.

3. Conclusions

In summary, we report the physical and chemical behavior of PURE-type dendrimers, a class of biocompatible and pH-dependent fluorescent dendrimers that can be used as an efficient platform for siRNA delivery. The intelligent skilled biomimetic material showed the ability to change its conformation via a dynamic back-folding mechanism in response to external pH. Their ability to cross the cell membrane was clarified and their action as nano-buffers in the endosome proposed. Our results indicate that PURE-G4 dendrimers compact and effectively deliver siRNA molecules into cells and can efficiently shutdown the expression of a specific gene. Moreover, the PURE-G4-siRNA dendriplex dramatically decline cell oxidative stress and cytotoxicity of the carrier system even at high concentrations when compared with PURE-G4. The absence of cytotoxicity combined with the high siRNA transfection efficiency and effective gene silencing capability may be explored as new gene delivery vectors for nano-therapeutics. In vivo studies are being developed in order to further corroborate the dendriplexes efficiency as gene silencing platforms.

4. Experimental

4.1 Materials

PURE-type dendrimers were synthesized in supercritical carbon dioxide as previously reported[15] using an adapted a high-pressure apparatus.[42,43] All reagents were purchased commercially and were used as received unless otherwise noted.

4.2. Methods

NMR experiments. The NMR spectra were recorded on Bruker ARX 400 MHz equipment. ^{1}H NMR chemical shifts are reported as δ (ppm= parts per million) relative to the residual solvent peak.

Dynamic Light Scattering. For particle size determination samples were analyzed through Dynamic Light Scattering - a nanoparticle analyzer from Horiba Scientific Nano Portica sz 100 at an angle of 90º and at 37 ºC. Samples with concentrations in the range 1-100 mg/mL were previously filtered through a 0.45 μm membrane. Diluted HCl solutions were used to study the pH influence on the particles size. The zeta potential of the dendriplex was measured at pH 7.4 using a concentration of 14 mg/mL.

Atomic Force Microscopy. AFM was performed on a Molecular Imaging Agilent (model 5100) system operating in non-contact mode. Silicon cantilevers having a constant force in the range of 1-5 N/m and a resonant frequency ranging between 50-70 kHz were used. All images were recorded with 256×256 pixels resolution. The AFM images were processed using second order plane fitting and second order flattens routines. The levelling routines were applied in order to remove the z offset between scan lines and the tilt and bow in each scan line. All AFM images were processed using the same levelling procedure with the final images indicating a flat planar profile. Gwyddion (version 2.25) software was used to process the AFM images.

Potentiometric titration. Potentiometric titrations were performed using a Crison Basic 20 pH meter and a Crison 52 09 pH electrode at room temperature (24 ± 0.1 ºC). 0.1 M NaCl solutions containing 3 mg/mL of PURE-G4 dendrimers were titrated by standard HCl (0.1 N).

UV-Vis spectroscopy. The UV-Vis spectra of the titrated samples were obtained in a UV-1700 PharmaSpec Spectrometer from Shimadzu with a scan rate of 300 nm/min at 25 ºC.

Rheological measurements. The rheological measurements were performed on a Bohlin Gemini HRnano rotational rheometer (Malvern Instruments, UK) at different temperatures using a cone/plate geometry of 1º, 20 mm. Steady state measurements were performed in a shear rate range of 1-1000 s^{-1}.

Agarose gel electrophoresis. 5 μL of loading dye (6×) were added to 15 μL of a PAMAM and PURE-G4 solution with a concentration of 14 mg/mL, and 12 μL of each sample were loaded onto a 2% agarose gel. Electrophorese was performed in Tris-Borate-EDTA (TBE) buffer (1×) at pH 8 (TBE buffer contains 89 mM Tris-base, 200 mM boric acid and 2 mM EDTA) at room temperature and 70 V for 30 min.

Polyurea dendriplexes preparation. Increasing amounts of polyurea dendrimer (0.01 to 7.5 mg/mL) were mixed with 10 nM of siRNA (Sense strand: 5'-GCAUGACCAACAAGAUGAAUU-3', Antisense strand: 3'-UUCAUCUUGUUGGUCAUGCUU-5'; Dharmacon, Thermo Scientific) in DEPC-treated water, and incubated at 37 ºC for 2 hours. Polyurea dendriplexes were then analyzed by

electrophoresis on a 2% (w/v) agarose gel (UltraPure™ Agarose, Invitrogen).

Gel electrophoresis mobility shift assays (EMSA). Agarose gels were prepared in Tris-Borate-EDTA (TBE) buffer (1×) at pH 8 (TBE buffer contains 89 mM Tris-base, 200 mM boric acid and 2 mM EDTA). GelRed (Biotium) was added at 5× of a stock solution of 10.000× in water. Suitable sized wells (50 µL), were formed by placing a comb in the center of the gel. After the formation of PURE-G4-siRNA dendriplexes, 5 µL of loading dye (10 mM Tris-HCl pH 7.6, 0.03% bromophenol blue, 0.03% xylene cyanol FF, 60% glycerol, 60 mM EDTA; Fermentas) was added to ensure proper well loading and a constant electric field (70 V) was applied for 45 min for sufficient separation, at room temperature. EMSA gels after electrophoresis were visualized under UV illumination and gel photographs were taken with a Gel Documentation EQ System (Biorad). The electrophoretic mobility (RF) values for PURE-G4 complexed with siRNA were determined as follows: RF= distance migrated/gel length.

Cell culture and dendrimer incubation. HepG2 cells (Human hepatocellular liver carcinoma cell line) were grown in Dulbecco's modified Eagle's medium with Glutamax (DMEM, Invitrogen) with 10% heat inactivated fetal bovine serum (Invitrogen), 100 U/mL penicillin and 100 µg/mL streptomycin (Invitrogen) and maintained at 37 ºC in 5% CO_2. Cells were also supplemented with 1× non-essential aminoacids (Sigma). Cells were seeded at a density of 1×10^5 cells/well in 24-well plates and grown for 24 h prior to transfection of the GFP vector (pVisionGFP-N vector 4.7 kb, Biovision) encoding for green fluorescent protein, VisionGFP, optimized for high expression in mammalian cells. On the day of transfection, EGFP vector (1 mg per well) was added to cells at approximately 50% confluence with 2 mg of Lipofectamine 2000® (Invitrogen) and Opti-MEM® Reduced Serum Medium (Invitrogen) according to the manufacturer's recommendations. On the day of dendrimer incubation, PURE-G4/siRNA complexes for 1, 2.5, 5 and 7.5 mg/mL of dendrimer pre-incubated with 10 µM of siRNA control or anti-GFP siRNA were added to cells (for 48 hours) that were at approximately 50% confluence. For comparison with dendriplex potency in silencing, Lipofectamine 2000® was also used to transfect anti-GFP and control siRNAs. Briefly, after 24 h of GFP transfection, cells were treated with 10 µM anti-GFP and control siRNAs using 1.5 mg of Lipofectamine 2000® (Invitrogen) and Opti-MEM® Reduced Serum Medium (Invitrogen) according to the manufacturer's recommendations. GFP silencing was evaluated at the protein level by measuring GFP fluorescence from cell lysates. Briefly, after 48 h, cells were washed with 1× PBS, lysed in water and collected for analysis of GFP silencing. Fluorescence was measured at least 3 times in a Cary Eclipse spectrofluorimeter (Varian) using an Ultra-Micro quartz cell (Hëllma) by taking the area under the curve from 495 to 650 nm. GFP fluorescence values were normalized to the bulk protein concentration determined via the Bradford assay (Thermo Scientific), and then normalized against the controls to determine percent knockdown of GFP. At the mRNA level, GFP expression was measured using Real-Time RT-PCR as described below.

Real-Time RT-PCR. Total RNA was extracted from the cell line using the Trisure reagent (Bioline) according to the manufacturer's protocol, and used for qRT-PCR to evaluate expression of GFP and β-actin. cDNA was attained by subjecting 1 µg of total RNA to Reverse Trancriptase with 200U of Revert-AidTM M-MuLV Reverse Transcriptase (Fermentas) according to the manufacturer's specifications, using 20 µM of GFP and β-actin reverse primers, annealing at 42 ºC for 1 h and 70 ºC for 10 min to reverse transcriptase inactivation. Real-Time PCR amplification was performed in a Corbett Research Rotor-Gene RG3000 using SYBR GreenER Real-Time PCR Kit (Invitrogen) according to manufacturer's specifications in 50 µl reactions containing 2 µl of cDNA, 1 × SYBR Green SuperMix and 200 nM of primers (STABVIDA, Portugal).

Confocal microscopy. All confocal microscopy samples were prepared as described above. During the final 45 minutes of the incubations, the lysosomal dye Lysotracker® Green DND26 (Invitrogen) was included at a final concentration of 62.5 nM. Cells were then fixed with 4% paraformaldehyde in 1× PBS for 15 min at 37 ºC and incubated with 50 mM NH_4Cl (that serves as uncoupler for blocking of free aldehyde groups and consequently quenching auto-fluorescence) for 15 min at 37 ºC. Finally, cells were mounted in glycerol 87%. Images of cells were taken with a Confocal Laser Point-Scanning Microscope Zeiss LSM 510 META. Once optimized, the same microscope settings were used throughout. For excitation laser lines were used at a wavelength of 405 nm for the dendrimers and 514 nm for Lysotracker®.

Statistical analysis. All statistical analysis were performed with SPSS statistical package (version 17, SPSS Inc., Chicago, IL) using a Paired-Sample T-test. All experiments, unless otherwise stated, were performed in triplicate. All error bars used in this report are ± s.d. of at least three independent experiments.

Acknowledgements

We acknowledge LabRMN at FCT/UNL and Rede Nacional de RMN for access to the facilities. Rede Nacional is supported with funds from Fundação para a Ciência e a Tecnologia (FC&T, Lisbon), Projecto de Re-equipamento Científico, Portugal. We thank the financial support from FC&T through Strategic Projects PEst-C/CTM/LA0025/2013, PEst-OE/SAU/UI0009/2013 and PEst-C/EQB/LA0006/2013 (FC&T: financial support to CENIMAT/I3N, CIGMH and REQUIMTE) and projects PTDC/EQU-EQU/116097/2009, PTDC/BBB-NAN/1812/2012, PTDC/CTM/099452/2008, PhD grants SFRH/BD/66858/2009 (R.B.R.) and SFRH/BD/62957/2009 (J.C.).

.

Notes and references

[a] REQUIMTE, Departamento de Química, Faculdade de Ciências e Tecnologia, Universidade Nova de Lisboa, Campus de Caparica, 2829-516 Caparica, Portugal.
[b] CIGMH, Departamento de Ciências da Vida, Faculdade de Ciências e Tecnologia, Universidade Nova de Lisboa, Campus de Caparica, 2829-516 Caparica, Portugal.
[c] Instituto de Nanociencia de Aragon, Universidad de Zaragoza, Zaragoza, Spain.
[d] Current address: Massachusetts Institute of Technology, Harvard–MIT Biomedical Engineering Center, E25-449, Cambridge, Massachusetts, USA.
[e] Departamento de Ciências dos Materiais e CENIMAT, Faculdade de Ciências e Tecnologia, Universidade Nova de Lisboa, Campus de Caparica, 2829-516 Caparica, Portugal.
[f] Instituto de Telecomunicações, Instituto Superior Técnico, Av. Rovisco Pais, 1049-001 Lisboa, Portugal.
[g] Departamento de Bioengenharia, Instituto Superior Técnico, Av. Rovisco Pais, 1049-001 Lisboa, Portugal.[h] CICS–UBI Health Sciences Research Center, University of Beira Interior, Avenida Infante D. Henrique, 6200-506 Covilhã, Portugal.
* Corresponding Authors: Tel. +351 212949648; Email: air@fct.unl.pt (A.A.-R.), vasco.bonifacio@tecnico.ulisboa.pt (V.D.B.B.).

† Electronic Supplementary Information (ESI) available: Atomic Force Microscopy; Viscosity of PURE-G4 versus shear rate; MTT assay of PURE-G4 and dendriplexes compared with the commercial delivery vector Lipofectamine; GFP silencing with siRNA transfected with Lipofectamine.. See DOI: 10.1039/b000000x/

1 F. Takeshita, T. Ochiya, *Cancer Sci.* 2006, **97**, 689–696.
2 J. C. Burnett, J. J. Rossi, K. Tiemann, *Biotechnol. J.*, 2011, **6**, 1130–1146.
3 J. B. Lee, J. Hong, D. K. Bonner, Z. Poon, P. T. Hammond, *Nat. Mater.*, 2012, **11**, 316–322.
4 A. Dillin, PNAS, 2003, **100**, 6289–6291.
5 B. Ozpolat, A. K. Sood, G. L. Berestein, *J. Intern. Med.,* 2009, **267**, 44–53.
6 R. Kanasty, J. R. Dorkin, A. Vegas, D. Anderson, *Nat. Mater.*, 2013, **12**, 967–977.
7 S. Trehan, G. Sharma, A. Misra. *Syst. Rev. Pharm.*, 2010, **1**, 1–16.
8 S.-T. Chou, Q. Leng, P. Scaria, J. D. Kahn, L. J. Tricoli, M. Woodle, A. J. Mixson, *Biomacromolecules*, 2013, **14**, 752−760.
9 J. F. G. A. Jansen, E. M. M. B.-v. den Berg, E.W. Meijer, *Science*, 1994, **266**, 1226–1229.
10 Dendrimers in medicine and biotechnology – New molecular tools (Eds: U. Boas, J. B. Christensen, P.M.H. Heegaard), The Royal Society of Chemistry, UK, 2006.
11 Dendrimer-based medicine (Eds: I.J. Majoros, J.R. Baker, Jr.), Pan Stanford Publishing, Singapore, 2008.
12 J. A. Barreto, W. O'Malley, M. Kubeil, B. Graham, H. Stephan, L. Spiccia, *Adv. Mater.*, 2011, **23**, H18–H40.
13 M. A. Mintzer, M. W. Grinstaff, *Chem. Soc. Rev.*, 2011, **40**, 173–190.
14 D. Astruc, E. Boisselier, C. Ornelas, *Chem. Rev.*, 2010, **110**, 1857–1959.
15 R. B. Restani, P. I. Morgado, M. P. Ribeiro, I. J. Correia, A. Aguiar-Ricardo, V. D. B. Bonifácio, *Angew. Chem. Int. Ed.*, 2012, **51**, 5162–5165.
16 S. Mitragoti, J. Lahann, *Nat. Mater.*, 2008, **8**, 15–23.
17 R. A. Petros, J. M. DeSimone, *Nat. Rev. Drug Discov.,* 2010, **9**, 615–627.
18 K. L. Wooley, C. A. Klug, K. Tasaki, J. Schaefer, *J. Am. Chem. Soc.*, 1997, **119**, 53–58.
19 C. B. Gorman, M. W. Hager, B. L. Parkhurst, J. C. Smith, *Macromolecules*, 1998, **31**, 815–822.
20 A. W. Bosman, M. J. Bruining, H. Kooijman, A. L. Spek, R. A. J. Janssen, E. W. Meijer, *J. Am. Chem. Soc.*, 1998, **120**, 8547–8548.
21 M. Chai, Y. Niu, W. J. Youngs, P. L. Rinaldi. *J. Am. Chem. Soc.*, 2001, **123**, 4670–4678.
22 K. X. Moreno, E. E. Simanek, *Macromolecules*, 2008, **41**, 4108–4114.
23 R. L. Lescanec, M. Muthukumar, *Macromolecules*, 1990, **23**, 2280–2288.
24 W. Chen, D. A. Tomalia, J. L. Thomas, *Macromolecules*, 2000, **33**, 9169–9172.
25 A. D. Meltzer, D. A. Tirrell, A. A. Jones, P. T. Inglefield, D. M. Hedstrand, D. A. Tomalia, *Macromolecules*, 1992, **25**, 4541–4548.
26 R. Esfand, D. A. Tomalia, *Drug Discov. Today*, 2001, **6**, 427–436.
27 J. Mattia, P. Painter, *Macromolecules*, 2007, **40**, 1546–1554.
28 C. Wu, J. Wang, P. Chang, H. Cheng, Y. Yu, Z. Wu, D. Donga, F. Zhao, *Phys. Chem. Chem. Phys.*, 2012, **14**, 464–468.
29 T. Müller, D. G. Yablon, R. Karchner, D. Knapp, M. H. Kleinman, H. Fang, C. J. Durning, D. A. Tomalia, N. J. Turro, G. W. Flynn, Langmuir, 2002, **18**, 7452–7455.
30 I. M. Klotz, V. H. Stryker, *J. Am. Chem. Soc.*, 1960, **82**, 5169–5172.
31 S. Akhtar, M. D. Hughes, A. Khan, M. Bibby, M. Hussain, Q. Nawaz, J. Double, P. Sayyed, *Adv. Drug Deliv. Rev.*, 2000, **44**, 3–21.
32 T. Niidome, L. Huang, *Gene Ther.,* 2002, **9**, 1647–1652.
33 I. R. Gilmore, S. P. Fox, A. J. Hollins, M. Sohail, S. Akhtar, *J. Drug Target*, 2004, **12**, 315–340.
34 F. R. Maxfield, D. Yamashiro, *J. Adv. Exp. Med. Biol.*, 1987, **225**, 189–198.
35 J. Huotari, A. Helenius, EMBO J., 2011, **30**, 3481–3500.
36 M. E. Davis, Z. Chen, D. M. Shin, *Nat. Rev. Drug Discov.*, 2008, **7**, 771–782.
37 C. E. Ashley, E. C. Carnes, G. K. Phillips, D. Padilla, P. N. Durfee, P. A. Brown, T. N. Hanna, J. Liu, B. Phillips, M. B. Carter, N. J. Carroll, X. Jiang, D. R. Dunphy, C. L. Willman, D. N. Petsev, D. G. Evans, A. N. Parikh, B. Chackerian, W. Wharton, D. S. Pea-body, C.J. Brinker, Nat. Mater., 2011, **10**, 389–397.
38 M. Dominska, D. M. Dykxhoorn, *J. Cell Sci.,* 2010, **123**, 1183–1189.
39 O. Taratula, O. B. Garbuzenko, P. Kirkpatrick, I. Pandya, R. Savla, V. P. Pozharov, H. He, T. Minko. *J. Control. Release*, 2009, **140**, 284–293.

40 J. Zhou, K. T. Shum, J. C. Burnett, J. J. Rossi, *Pharmaceuticals*, 2013, **6**, 85–107.
41 J. Conde, J. Rosa, J. M. de la Fuente, P. V. Baptista, *Biomaterials*, 2013, **34**, 2516–2523.
42 C. Veiga de Macedo, M. Soares da Silva, T. Casimiro, E. J. Cabrita, A. Aguiar-Ricardo, *Green Chem.,* 2007, **9**, 948–953.
43 V. G. Correia, V. D. B. Bonifácio, G. Moutinho-Fragoso, T. Casimiro, C. Lobato da Silva, M. G. Pinho, A. Aguiar-Ricardo, *Macromol. Biosci.,* 2011, **11**, 1128–1137.